JBIC Journal of Biological Inorganic Chemistry (2022) 27:373–389
https://doi.org/10.1007/s00775-022-01936-5

ORIGINAL PAPER

Conjugation of triphenylantimony(V) with carvacrol against human breast cancer cells

Marianthi Kapetana[1] · Christina N. Banti[1] · Christina Papachristodoulou[2] · Vassilios Psycharis[3] · Catherine P. Raptopoulou[3] · Sotiris K. Hadjikakou[1,4]

Received: 6 January 2022 / Accepted: 21 February 2022 / Published online: 17 March 2022

Abstract

The organoantimony derivative of formula *trans*-O,O-[$Ph_3Sb^V(Carv)_2$] (**TPAC**) (CarvH = carvacrol) is obtained by the oxidation of triphenylstibine (Ph_3Sb^{III}) with hydrogen peroxide in the presence of carvacrol (CarvH). Physical methods such as X-ray Fluorescence (XRF) spectroscopy, single crystal and powder X-ray diffraction analysis (XRD and PXRD), Attenuated Total Reflection Fourier Transform Infra-red (ATR-FTIR) spectroscopy, Thermogravimetric Differential Thermal Analysis (TG–DTA) and Differential Scanning Calorimetry (DTG/DSC), confirm the retention of the formula of **TPAC** throughout the sample mass in solid state, while UV–Vis spectroscopy in the solution. **TPAC** is the first example of carvacrol (the main ingredient of oregano) covalently bonded to any metal ion. Only the *trans*-O,O-[$Ph_3Sb(Carv)_2$] isomer was isolated suggesting stereo-selectivity of the preparation route. **TPAC** inhibits in vitro both human breast adenocarcinoma cell lines: MCF-7 (positive to hormones receptor (HR +)), MDA-MB-231 (negative to hormones receptor (HR-)) stronger than normal human fetal lung fibroblast cells (MRC-5). The MCF-7 cells morphology, DNA fragmentation, Acridine Orange/Ethidium Bromide (AO/EB) Staining, cell cycle arrest and mitochondrial membrane permeabilization tests suggest an apoptotic pathway for cell death, especially, through the mitochondrion damage. The binding type of **TPAC** toward the calf thymus CT-DNA was initially deduced ex vivo from the differentiation of the DNA solution viscosity. Fluorescence spectroscopy confirms the interaction mode suggested. Spectroscopic evidence (FTIR, UV–Vis) suggest that glutathione (GSH) (a tripeptide overexpressed in tumor cells) induces conversion of non-active pentavalent antimony, which is contained in **TPAC,** to active trivalent one, providing a new strategy for the development of targeted chemotherapeutics.

✉ Christina N. Banti
cbanti@uoi.gr

✉ Sotiris K. Hadjikakou
shadjika@uoi.gr

[1] Section of Inorganic and Analytical Chemistry, Department of Chemistry, University of Ioannina, 45110 Ioannina, Greece

[2] Department of Physics, University of Ioannina, 45110 Ioannina, Greece

[3] Institute of Nanoscience and Nanotechnology, National Center for Scientific Research "Demokritos", 15310 Athens, Greece

[4] Institute of Materials Science and Computing, University Research Center of Ioannina (URCI), 45110 Ioannina, Greece

Graphical abstract

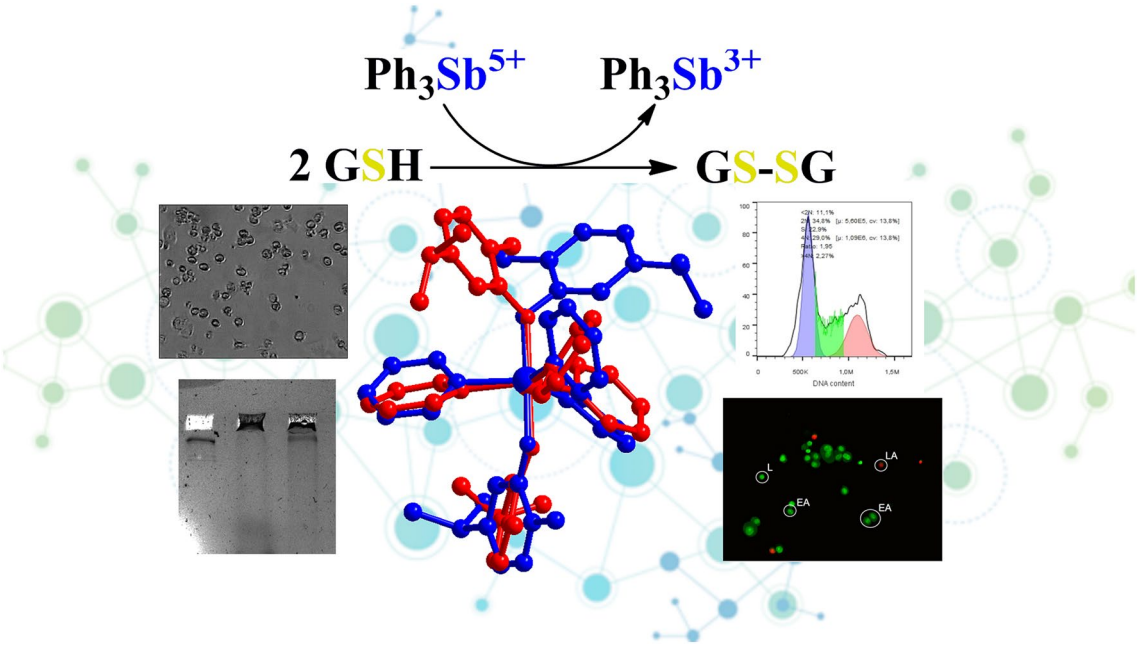

Keywords Biological inorganic chemistry · Pentavalent antimony metallodrugs · Carvacrol · Natural product · Cytotoxicity · Apoptosis

Introduction

Carvacrol, a monoterpenoid phenol, found in oregano exhibits antimicrobial, insecticidal, anti-angiogenic, and antitumor biological activities [1]. Especially, the antiproliferative activity of carvacrol against non-small cell lung cancer cells, chronic myeloid leukemia cells, murine melanoma cells and metastatic breast cancer, MDA-MB-231 cells ($IC_{50} = 100$ µM) is already reported [2, 3]. Carvacrol induces apoptosis, cell cycle arrest at S phase, increases caspase activity, releases cytochrome c from mitochondria, decreases mitochondrial membrane potential and induces DNA fragmentation [2, 3]. Antimony, on the other hand, is used in medicine, against microbes and parasites [4–8]. Pentavalent antimonials are used as antileishmanial drugs, for a long time now [9]. In these formulations, antimony(V) is acting as pro-drug that is converted to active antimony(III) ones by the tripeptide glutathione (GSH) [4, 9]. It is noted that Sb(V) is biologically low active, while Sb(III) is the active form of antimonials [4–6]. Recently, antimony(III) compounds were studied for in vitro antiproliferative activity which, in some cases, is higher than the corresponding one of cisplatin, doxorubicin or tamoxifen drugs [4–8, 10–13]. Moreover, GSH is over-expressed in tumor cells, (e.g., its concentration is twice in breast cancer cells than that

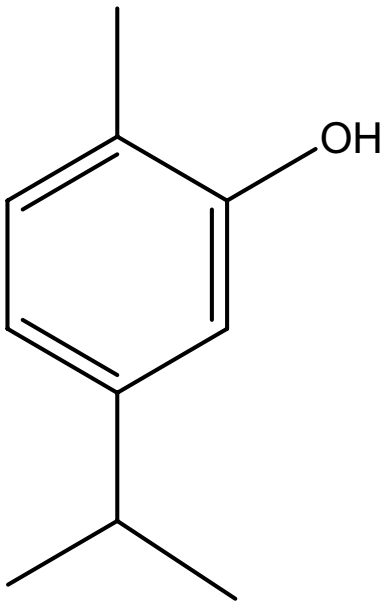

Scheme 1 Molecular structure of CarvH

found in normal ones), and it involves in multidrug resistance of tumor cells through its spontaneous reaction with anticancer drugs, such as cisplatin [14, 15]. Therefore, the use of low active Sb(V) species which are converted to the active Sb(III) ones inside to cancer cells by the GSH is expected to lead in new chemotherapeutics with high selectivity against cancer cells than normal ones.

The antitumor activity of organoantimony(III) compounds, on the other hand, was reported for the first time during 1990s, [16]. Later on, the relatively high antitumor activity of organoantimony(V) compounds was reported as well [8, 17]. So far, the most studied antimony compounds in the context of antitumor activity are organometallic. Therefore, the study of new organoantimony compounds for the purpose of developing anticancer drugs is meaningful.

In the course of our studies for the development of new targeted metallotherapeutics [4–8, 10–13, 15, 18–24], with enhanced biological activity**,** capable of overcoming tumor cells resistance, the *trans*-O,O-[$Ph_3Sb(Carv)_2$] (CarvH = carvacrol, Scheme 1) (**TPAC**) was synthesized and characterized by m.p, XRD, XRF, FTIR, PXRD, TG–DTA, DTG/DSC and UV–Vis spectroscopies. The crystal structure of **TPAC** was also determined by X-ray crystallography. The in vitro activity of **TPAC** against breast cancer cells was evaluated, while its mechanism of action was clarified by ex vivo studies**.** The GSH conversion of non-active pentavalent antimony, which is contained in **TPAC,** to active trivalent one, is also studied spectroscopically.

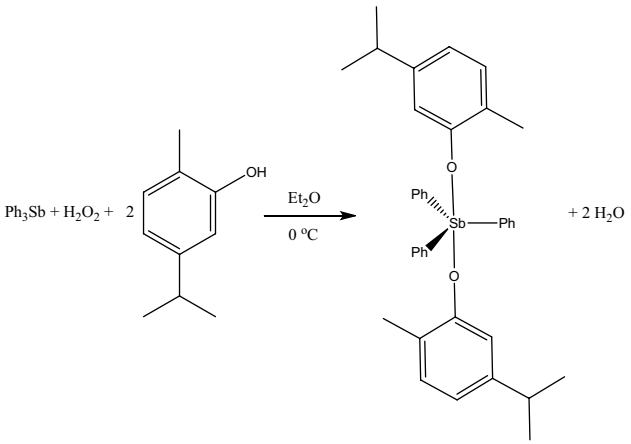

Scheme 2 Synthesis of **TPAC**

Results and discussion

General Aspects: **TPAC** is obtained by the oxidation of triphenystibine ($Ph_3Sb(III)$) with hydrogen peroxide in the presence of carvacrol (CarvH) (Scheme 2). The white precipitation of the reaction was filtered off and dried. Colorless crystals of **TPAC** were grown by slow evaporation of methanol/acetonitrile solution of the product. The formula of **TPAC** was initially determined with spectroscopic methods.

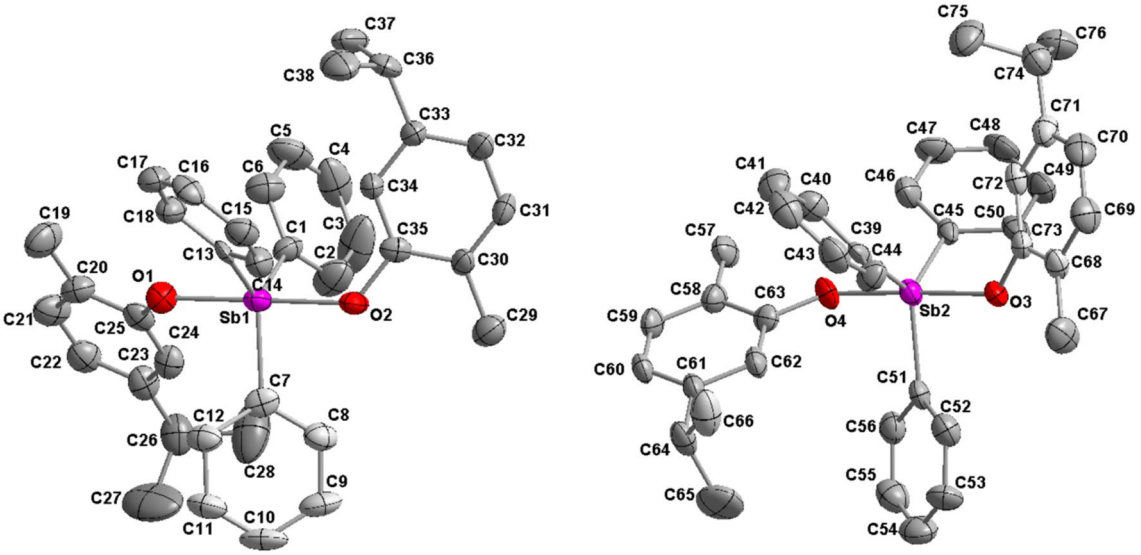

Fig. 1 ORTEP-labeled plots of the two symmetry independent isomers (**A** and **B**) with the thermal ellipsoids at 50% probability for **TPAC**. Selected bond lengths (Å) and angles [°]; isomer **A** Sb1–O1 = 2.048(6), Sb1–O2 = 2.054(6), Sb1–C1 = 2.095(9), Sb1–C7 = 2.089(8), Sb1–C13 = 2.100(8), O1–Sb1–O2 = 179.5(2), O1–Sb1–C1 = 91.5(3), O1–Sb1–C7 = 94.1(3), O1–Sb1–C13 = 85.7(3), O2–Sb1–C1 = 88.9(3), O2–Sb1–C7 = 85.5(3), O2–Sb1–C13 = 94.2(3), C1–Sb1–C7 = 120.3(3), C1–Sb1–C13 = 123.1(3), C7–Sb1–C13 = 116.6(3); isomer **B** Sb2–O4 = 2.037(6), Sb2–C39 = 2.112(8), Sb2–O3 = 2.049(6), Sb2–C45 = 2.104(9), Sb2–C51 = 2.111(8), O3–Sb2–C45 = 94.8(3), O3–Sb2–C51 = 86.3(3), O4–Sb2–C39 = 91.0(3), O4–Sb2–C45 = 85.2(3), O4–Sb2–C51 = 91.9(3), O3–Sb2–C39 = 90.8(3), O3–Sb2–O4 = 177.9(2), C39–Sb2–C45 = 121.6(3), C39–Sb2–C51 = 117.0(3), C45–Sb2–C51 = 121.4(3)

The structure was refined by single crystal X-ray diffraction analysis. The crystals are air stable when they are stored in the darkness at room temperature. The compound is soluble in n-hexane, methanol, acetonitrile and DMSO.

Solid-state studies

Crystal and molecular structure of ***TPAC***: ORTEP diagram of **TPAC** along selected bond lengths and angles are listed in Fig. 1. Although there are three crystal structures where carvacrol coexists with metal ions reported up to now [25–27] the crystal structure **TPAC** is the first example one where carvacrol is covalently bonded to any metal. The reported structures include those where carvacrol is co-crystallized in the crystal lattice: the catena-[tetrakis(μ-2,4,6-tris(pyridin-4-yl)-1,3,5-triazine) dodecabromohexa-zinc 5-isopropyl-2-methylphenol] [25], and catena-[sesquikis[(μ-*N*,*N*′′-(biphenyl-4,4′-diyl)diisonicotinamide)-bis(μ-biphenyl-4,4′-dicarboxylato)-di-zinc(ii)] (eugenol) (carvacrol) clathrate N,Ndimethylformamide] [26] and the structure of the organometalic compound (η^5-Pentamethyl-cyclopentadienyl)-(η^6-2-hydroxy-p-cymene)-ruthenium trifluoromethanesulfonate [27].

There are two isomers (A and B) in the asymmetric unit (Fig. 1). Based on the overlay diagram of the symmetry independent molecules (Figure S1) and their respective torsion angles of the core structure of the two isomers (Fig. 1), these differ in the orientation of one of the two deprotonated carvacrol ligands, defined by O1, C19, C28 and O3, C67, C76 for the those contains the Sb1 and Sb2 cations, respectively (Figure S1). The coordination polyhedron for both Sb1 (isomer A) and Sb2 (isomer B) atoms is trigonal bipyramids. Three carbon atoms from the phenyl groups form the equatorial plane, while two oxygen atoms from two ligands occupy the axial positions (Sb1–O1 = 2.048(6), Sb1–O2 = 2.054(6), Sb2–O4 = 2.037(6) and Sb2–O3 = 2.049(6) Å) forming a *trans*-O,O-[$Ph_3Sb(Carv)_2$] conformation. Both hydroxyl groups of carvacrol have been deprotonated during the oxidation process of Sb(III) to Sb(V). According to Reedijk, the parameter $\tau = (b-a)/60$ (where b = the largest angle around Sb(V), a = the second largest one) tends to zero in the case of tetragonal pyramidal geometry, while in the ideal trigonal bipyramidal one is equals to unity [28, 29]. In the case of the isomer A, the angles $b = 179.5(2)°$ (O1–Sb1–O2) and $a = 123.1(3)°$ (C1–Sb1–C13) (Fig. 1) lead to τ value of 0.94 which indicates an ideal TBP arrangement around Sb. In the case of the isomer B, the angles $b = 177.9(2)°$ (O3–Sb2–O4) and $a = 121.6(3)°$ (C39–Sb2–C45) (Fig. 1) lead to τ value of 0.94 as well. Quit few reports with crystal structures of *trans*-O,O- or *cis*-O,O- triphenyl antimony derivatives of alcohols are found in the literature. These include those with *trans*-O,O- arrangement: *trans*-O,O-[(p-Me-Ph)$_3$Sb(2,4,6-tribromophenolato)] [30], *trans*-O,O-[(p-F-Ph)$_3$Sb(4-nitrophenolato)] [31], *trans*-O,O-[Ph_3Sb(4-iodophenolato)] [32], *trans*-O,O-[Ph_3Sb(phenolato)] [33], structures with *cis*-O,O- arrangement include *cis*-O,O-[Ph_3Sb(2,2′-Iminobis(4,6-di-t-butylphenolato))] [34]. Only the *trans*-O,O-[$Ph_3Sb(Carv)_2$] isomer was isolated in the case of **TPAC** suggesting stereo-selectivity of the preparation route.

Both complexes form a 1D polymeric assembly through π···π and C–H···π interactions (Figure S2).

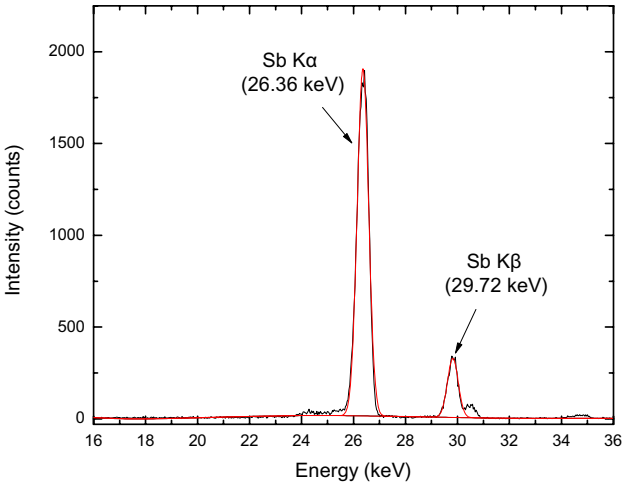

Fig. 2 XRF spectrum of **TPAC**. The Sb Kα radiation was used for quantitative determination of Sb in the samples

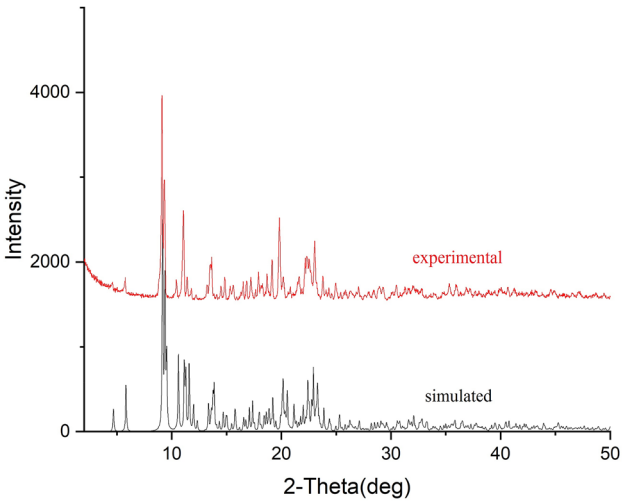

Fig. 3 The simulated XRPD pattern using single crystal XRD data, which is overlaying the experimental one, adequately resembles the experimental pattern

X-ray fluorescence spectroscopy (XRF): The XRF spectrum of **TPAC** (powder) confirms the presence of Sb (Fig. 2). The content of **TPAC** in Sb is 22 ± 3% w/w, while the calculated one is 19% w/w confirming the *trans*-O,O-$[Ph_3Sb(Carv)_2]$ composition of the bulk of the sample.

Vibrational spectroscopy: The vibration band at 3367 cm^{-1} in the IR spectrum of CarvH is attributed at the –OH group [35]. No such vibration is observed in the IR spectrum of **TPAC** (Figure S3), indicating the coordination of CarvH to the Sb(V) ion through the –OH group. The vibration band at 1251 cm^{-1} in the IR spectra of CarvH and **TPAC**, is attributed in the C–O bond vibration. The corresponding vibration bands for the $C_{(aromatic)}$–H and $C_{(aliphatic)}$–H are observed at 3063 and 2960 cm^{-1}, respectively, in both spectra (CarvH and **TPAC**). Moreover, the vibration band of Sb–O in the IR spectrum of **TPAC** appears at 620 cm^{-1} [36].

X-ray powder diffraction (PXRD) analysis. The PXRD spectrum of the powder of **TPAC** is identical to the simulated one which is derived using single crystal XRD data (Fig. 3). In conclusion, the purity of the sample was also proven by (i) the X-ray fluorescence spectroscopic data where the antimony content in the sample (~ 10 mg) measured corresponds to the proposed formula and (ii) the vibrational spectroscopic data where the assignment of the ATR-FT-IR spectrum has been based on its crystal structure.

Thermo-gravimetric analysis of TPAC

*Thermal decomposition of **TPAC**:* TG/DTA analysis was performed using dry powder of TPAC, with temperature rate 10 °C min^{-1} from ambient up to 500 °C (Figure S4). **TPAC** decomposes with three endothermic steps (110–200 °C, 200–325 °C and 325–514 °C) (Figure S4) with total mass loss of 85%.

Differential scanning calorimetry (DSC): The DSC thermodiagram of **TPAC** (Figure S4) is dominated by two endothermic transitions which are observed at 277.0 and 513.9 °C, respectively.

Solution stability studies

The stability of **TPAC** in DMSO and in Phosphate Buffer (PBS) Solutions was tested by UV–Vis spectra for a period of 48 h (Figure S5). The duration of 48 h for the stability was chosen because this is the required cell culture incubation period in the biological experiments. No changes were observed between the initial UV–Vis spectra and those after 48 h confirming the retention of the structure in both solutions (DMSO and PBS).

Biological tests

Cisplatin, a well-known antiproliferative drug of clinical use, carvacrol, a natural product which induces apoptosis, increases caspase activity, releases cytochrome c from mitochondria, decreases mitochondrial membrane potential and induces DNA fragmentation [2, 3] and the Ph_3Sb have been used as positive and negative control compounds for the biological studies.

*Antiproliferative activity of **TPAC**:* Since, both constituents of **TPAC,** i.e., antimony(III) [4–6] and carvacrol exhibit antiproliferative effects which in the case of CarvH includes metastatic breast cancer cells, MDA-MB231 (HI), [2, 3], **TPAC** was tested against this cell line. As the hormone receptors on the other hand, are involved in the development and propagation of the cancer [37], MCF-7 (HD) cells were used as well. The antiproliferative activity (IC_{50}) of TPAC against cancer cells was evaluated by Sulforhodamine B (SRB) assay upon their incubation for 48 h (Table 1).

The IC_{50} values of **TPAC** against MCF-7 (HD) and MDA-MB-231 (HI) cells are 7.1 ± 0.2 and 7.2 ± 0.3 μM, respectively. Thus, **TPAC** inhibits both MCF-7 (HD) and MDA-MB-231 (HI) cells in similar manner. Given that both cell lines originate from the same tissue (breast), the hormones receptors play no role in the **TPAC**'s antiproliferative mechanism of action. The corresponding IC_{50} values of cisplatin are 5.5 ± 0.4 and 26.7 ± 1.1 μM against MCF-7 (HD) and MDA-MB-231 (HI) cells (Table 1). Compared to cisplatin, **TPAC** exhibits fourfold stronger activity against

Table 1 Antiproliferative activity of agents derived from the conjugation of natural ingredients with Sb(V) against MCF-7 (HD), MDA-MB 231 (HI) and MRC-5 cells

Compounds	IC_{50} (μM)			TPI		Refs.
	MCF-7	MDA-MB 231	MRC-5	MCF-7	MDA-MB 231	
$[Ph_3Sb(Carv)_2]$ (**TPAC**)	7.1 ± 0.2	7.2 ± 0.3	8.1 ± 0.3	1.1	1.1	*
$\{[Ph_3Sb(SalH)]_2O\}$	11.9 ± 0.6	8.0 ± 0.4	7.8 ± 0.2	0.7	1.0	[39]
CarH	> 30	> 30	> 30			*
Ph_3Sb	> 30	> 30	> 30			[40]
Cisplatin	5.5 ± 0.4	26.7 ± 1.1	1.1 ± 0.2	0.2	0.04	[40]

Cisplatin is used for comparison

*In this work, $salH_2$ = salicylic acid

MDA-MB-231 (HI) and it is less active towards MCF-7 (HD) (0.8-fold). Moreover, a selectivity of **TPAC** against both tumor cell lines than against normal ones was detected. Thus, the IC_{50} value of **TPAC** against MRC-5 cells is raised up to 8.1 ± 0.3 µM. This leads to therapeutic potency index (TPI) above 1 (TPI = 1.1 for both MCF-7 and MDA-MB-231 cells). FDA defines an agent with no selectivity when it exhibits MTC/MEC value less than 2 (MTC = minimum toxic concentration and MEC = minimum effective concentration [38]. TPI is defined as the IC_{50} of an agent against non-cancerous cells (MTC) towards its IC_{50} against cancerous cells (MEC) [20].

Table 1 summarizes the anti-proliferative activity of the organoantimony(V) derivatives with natural products ingredients such as salicylic acid (willow) or carvacrol (oregano). Among them, **TPAC** possesses more potent activity (IC_{50}) than {$[Ph_3Sb(SalH)]_2O$} ($SalH_2$ = salicylic acid) [39] against cancer cells (MCF-7 cells: 7.1 ± 0.2 µM (TPAC), 11.9 ± 0.6 µM ({$[Ph_3Sb(SalH)]_2O$}) and MDA-MB-231 cells: 7.2 ± 0.3 µM (**TPAC**), 8.0 ± 0.4µM ({$[Ph_3Sb(SalH)]_2O$}) (Table 1). Whilst {$[Ph_3Sb(SalH)]_2O$} exhibits low selectivity for tumor cells (TPI < 1) (Table 1).

In vitro mechanism of action

The in vitro mechanism of action of **TPAC** is evaluated by the (i) MCF-7 cells morphology, (ii) DNA fragmentation, (iii) Acridine Orange/Ethidium Bromide (AO/EB) Staining, (iv) cell cycle arrest and (v) mitochondrial membrane permeabilization tests.

Cell Morphology Study: The type of MCF-7 cell death upon their incubation with **TPAC** at the IC_{50} value for a period of 48 h, was firstly assessed, by the morphology of MCF-7 cells using phase contrast microscope (Fig. 4). The untreated MCF-7 cells maintained their morphology, as a result they are elongated, adherent and showed cellular crowding, suggestive of a normal proliferation. Incubated MCF-7 cells with **TPAC**, on the other hand, displayed morphological changes such as are rounded, were shrunk, lose contact with neighboring cells, were detached from the plate and they formed islets of rounded cells [23, 40]. These types of morphological changes of the MCF-7 cells suggest an apoptotic type of cell death when incubated with **TPAC**. To ensure this observation, the morphologies of MCF-7 cells incubated with **TPAC** are compared to those observed when cisplatin is used [40]. The similarity of the morphologies further suggests apoptotic cell death of MCF-7.

DNA fragmentation study: DNA fragmentation is a characteristic of apoptosis. This is because the formation of oligo

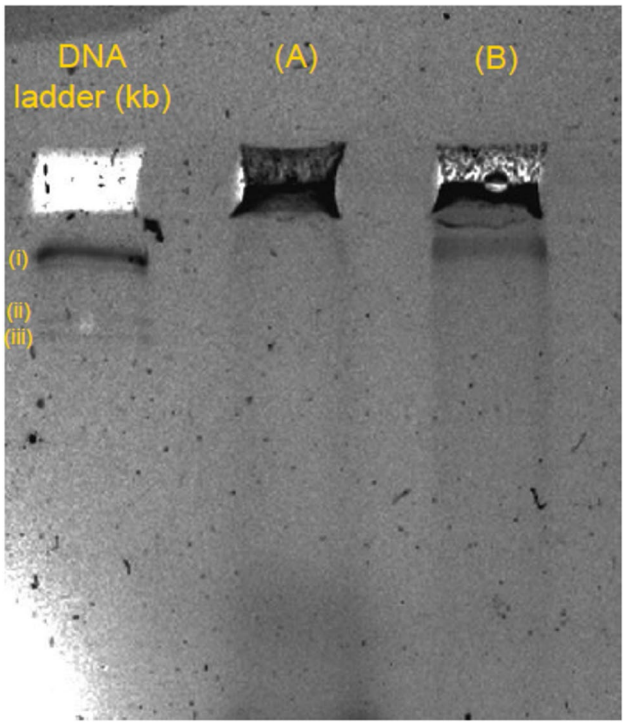

Fig. 5 DNA electrophoresis of MCF-7 cells incubated with **TPAC** for 48 h. DNA ladder 23,130 kb (i), 2,322 kb (ii), 2,027 kb(iii), control (**A**); incubated with **TPAC** (**B**)

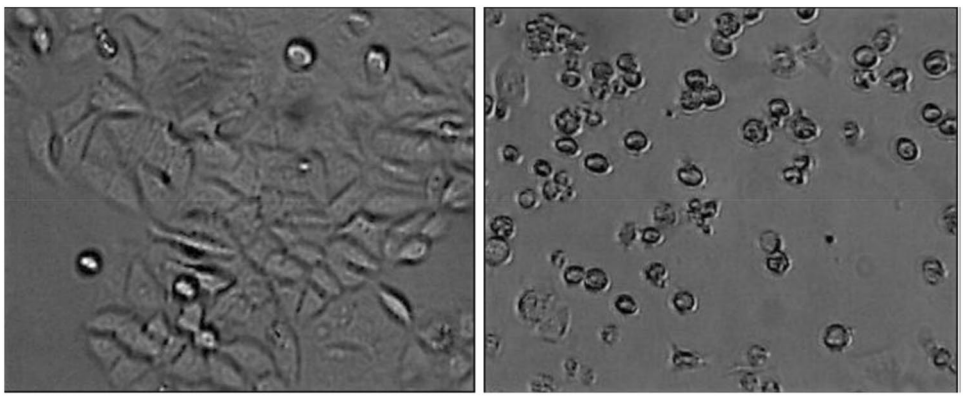

Fig. 4 Morphology of the untreated MCF-7 cells (**A**) and their alterations observed in the case of treated ones with **TPAC** (**B**) at its IC_{50} value for 48 h

nucleosomal-shaped rubbles from the chromosomal DNA cleavage in is a primary part of apoptosis [41]. To verify the apoptotic type of MCF-7 cell death when they are treated with **TPAC**, DNA fragmentation study was performed (Fig. 5). **TPAC** like cisplatin caused DNA laddering, which is a typical pattern of internucleosomal fragmentation [40], suggesting the apoptotic activity of the complex, in contrast to the untreated cells.

Acridine Orange/Ethidium Bromide (AO/EB) staining to detect apoptosis: The induction of apoptosis towards MCF-7 cell line was also tested by means of acridine orange (AO)/ethidium bromide (EB) staining followed by morphological analysis of nuclei after the exposure to **TPAC** in its IC_{50} value (Fig. 6).

This assay detects nuclear changes and apoptotic body formation that are characteristic of the cascade of apoptosis [42]. The fluorescent dye AO stains nuclear DNA in both live and dead cells. The fluorescent dye EB, on the other hand, stains, only, nuclear DNA in cells that have lost their membrane integrity [43]. The cells are classified to four types, according to the fluorescence emission and the morphological features of the stained nuclei (i) viable cells are uniformly stained green, (ii) early apoptotic cells are stained greenish yellow or displayed green yellow fragments, (iii) late apoptotic cells are stained orange or displayed orange fragments, and (iv) necrotic cells show orange to red fluorescing nuclei with no indication of chromatin fragmentation, uniformly red fluorescing, and the cells were swollen to large size [43].

In the case of the untreated MCF-7 cells, the cells are identified by bright uniform green nuclei with organized structures (Fig. 6). The percentage of apoptosis and necrosis in the control group was calculated 22.2 ± 4.9% and 0%, respectively. In the case of the incubated cells with **TPAC**, shrinkage is observed and chromatin condensation indicating that the majority of the cells undergoes apoptotic cell death (Fig. 6) [44]. The percentage of apoptotic and necrotic cells upon treatment in the case of **TPAC** is 43.3 ± 6.3%

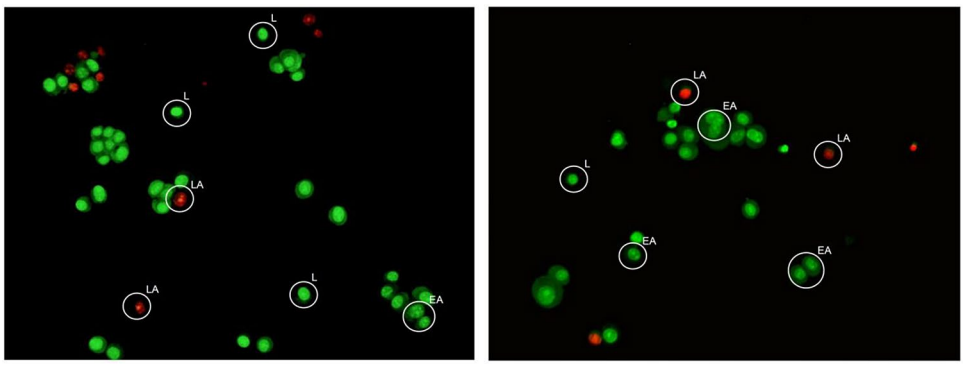

Fig. 6 Fluorescence images of the untreated MCF-7 cells (**A**) and treated ones with **TPAC** (**B**) for 48 h 37 °C at IC_{50} value and stained with acridine orange and ethidium bromide (AO/EB). ("L" indicates live cells; "EA" indicate early apoptotic cells; "LA" indicates late apoptotic cells)

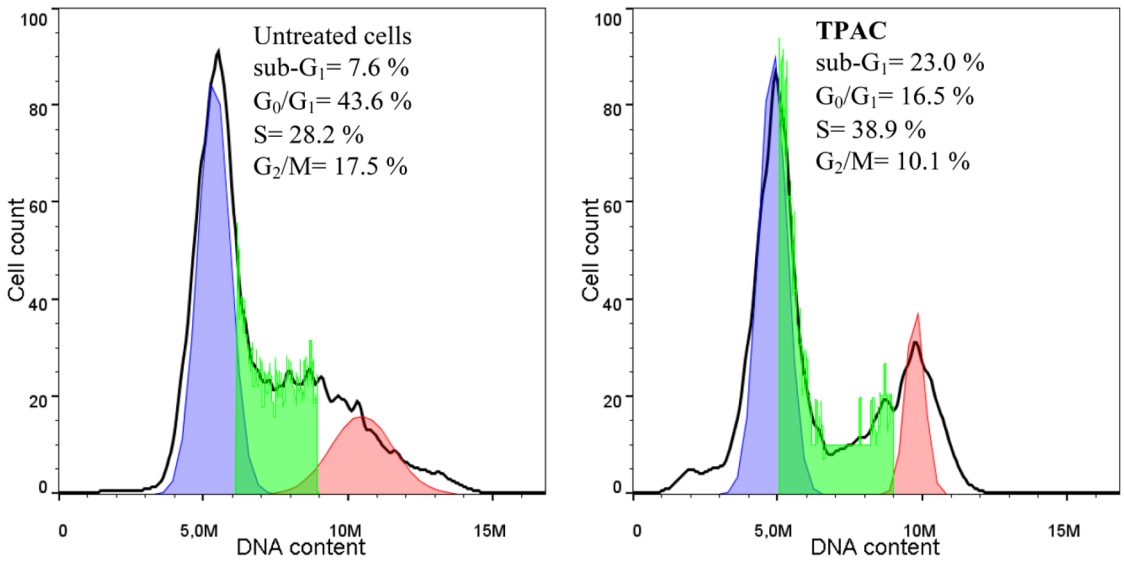

Fig. 7 Effect of **TPAC** on MCF-7 cell cycle. The relative number of cells within each cell cycle was determined by flow cytometry. Number of cells in sub-G_1, G_0/G_1, S and G_2/M phases are indicated

and 0%, respectively. When, MCF-7 cells are incubated with cisplatin, the percentage of apoptotic cells ends up to 96.5% [20, 22]. Therefore, the apoptotic type for the cell death is concluded to be induced by **TPAC**.

Cell cycle arrest study: To confirm, further, the apoptotic type of MCF-7 cell death upon their treatment with **TPAC** cell cycle studies were employed. MCF-7 cells were treated for 48 h with TPAC at the IC_{50} value, stained with propidium iodide (PI), and the amount of DNA was analyzed by flow cytometry. The results are presented in the DNA frequency histograms as the number of cells versus DNA content in different phases of cell cycle (sub-G_1, G_0/G_1, S, and G_2/M) (Fig. 7).

The percentage of untreated MCF-7 cells in the sub-G_1, G_0/G_1, S and G_2/M phases is 7.6%, 43.6%, 28.2% and 17.5%, respectively. However, the percentage of the treatment of MCF-7 cells with **TPAC**, in the sub-G_1 phase, is increased at 23.0% indicating an increase in the number of apoptotic cells [20, 23, 40]. Moreover, the percentage of the treated MCF-7 cells at S phase, increases at 38.9%, in contrast to the untreated cells (28.2%), suggesting that **TPAC** suppresses the cell proliferation due to DNA synthesis inhibition [40]. Cisplatin and carvacrol induce cycle arrest at S phase as well [2, 3, 40]. Therefore, **TPAC** causes apoptosis to MCF-7 cells in a similar manner to cisplatin and carvacrol.

Loss of the mitochondrial membrane permeabilization: Many metallodrugs are causing mitochondrial membrane permeability (MMP) dysfunction [19, 20, 23, 39, 40]. The mitochondrion is an essential component of the intrinsic apoptotic pathway and in the case of damaged of mitochondrion membrane integrity, the apoptotic factors are released initiating the cell death signaling [19, 20, 23, 39, 40]. The MMP assay is based on the cationic hydrophobic mitochondrial potential dye which is accumulated in mitochondria [19, 20, 23, 39, 40]. In the case of mitochondrion membrane dysfunction, the MMP collapses and the fluorescence emitted is simultaneously quenched. Upon treatment of MCF-7 cells with **TPAC**, the emitted light from the dye is quenched by 61.0%. Cisplatin, which is known to interact with mitochondria membrane, causes a quenching of only 54.9% when MCF-7 cells are treated with it [19, 40, 45]. Moreover, carvacrol induces apoptosis via the mitochondria-mediated pathway as well [46]. Therefore, an apoptotic type of MCF-7 cells death through loss of mitochondrion membrane permeability is concluded for **TPAC** following the behavior of both cisplatin and carvacrol.

Ex vivo mechanism of action

To investigate whether the Sb(V) compounds can be used as pro-drugs for targeted chemotherapy which are turning to active Sb(III) in the cytoplasm using the defending system of cancerous cells against chemotherapeutics, the GSH-induced conversion of Sb(V) (**TPAC**) to Sb(III) is studied here. Moreover, the apoptotic mechanism of cell death induced by **TPAC** was ex vivo studied by its interaction with CT-DNA. This study includes (i) DNA solution viscosity measurements and (ii) study of the quenching of fluorescence emitted by DNA–EB.

*GSH-induced conversion of Sb(V) (**TPAC**) to Sb(III)*: GSH is a tripeptide that is over-expressed in tumor cells and it involves in the development of cancer cells resistance to chemotherapeutics drugs. The low activity antimonials(V) pro-drugs, such as **TPAC**, on the other hand, can readily converted to the active drugs Sb(III) by GSH. Therefore the redox reaction between the GSH and **TPAC** is studied, here, using vibrational spectroscopy.

The ν(S–H) vibrational band in the ATR-FTIR spectrum of GSH (Figure S6) is absent when it oxidazes by H_2O_2 (1:1 molar ratio) due to the formation of the disulfide GS-SG formation (Figure S6) [47]. When **TPAC** is used instead of H_2O_2 under the same reaction conditions the ν(S–H) vibrational band is also absent from the spectrum of the resulting mixture (Figure S6) suggesting the oxidation of the GSH to the corresponding disulfide. Simultaneously the Sb(V) is reduced to Sb(III).

The redox reaction between GSH and **TPAC** is summarized in Eq. 1

$$2GSH + Ph_3Sb(Carv)_2 \rightarrow GS - SG + Ph_3Sb + 2CarvH. \quad (1)$$

The order of the reaction between **TPAC** with glutathione (GSH) was determined by UV spectroscopy. The initial UV spectra of the solutions (of final volume of 2.0 ml) containing different concentrations of **TPAC**, 33 (A), 66 (B) and 132 (C) μM in 100 mM Tris–HCl, pH = 7.4 with a high excess of GSH (16.5 mM) (1:500, 1:250 or 1:125 TPAC: GSH molar ratio) at 37 °C and after 1–6 h with 1-h interval are shown in Fig. 8. The increasing in absorption intensity of the solution at λmax = 270 nm with time is due to the reaction of metal complex with GSH (Fig. 8). However, as the rate of disulfide formation is low, the concentration of GSH was assumed not to change much over the time course due to the GSH-complex reaction. Because the GSH concentration is 500, 250 or 125 fold higher than that of **TPAC**, their reaction does not deplete GSH. The absorbance associated with GSH-complex reaction is obtained, by subtracting the absorbance due to the disulfide formed with the absent of the oxidizing agent (here **TPAC**) from the observed absorbance and the corresponding one of the complex alone (Fig. 9). The remaining absorbance at 270 nm is due to the formation of the product.

The initial rate of the reaction between GSH and a metallotherapeutic agent is calculated as described previously

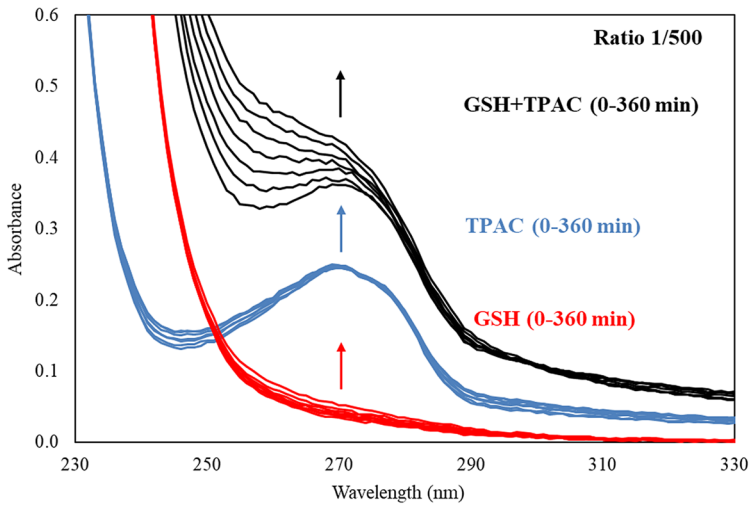

(A)

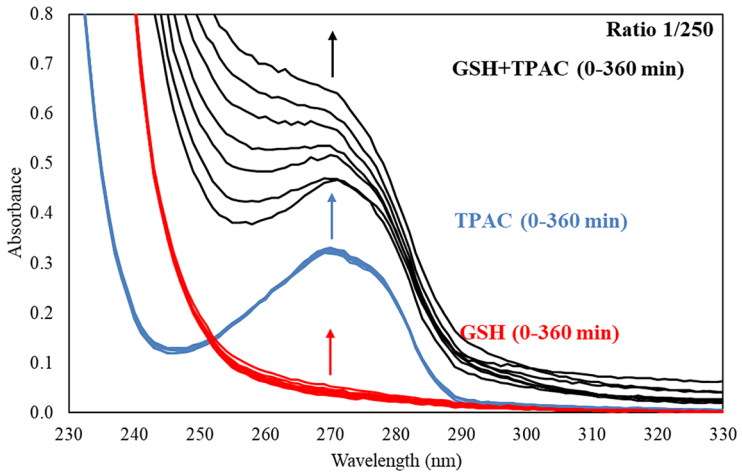

(B)

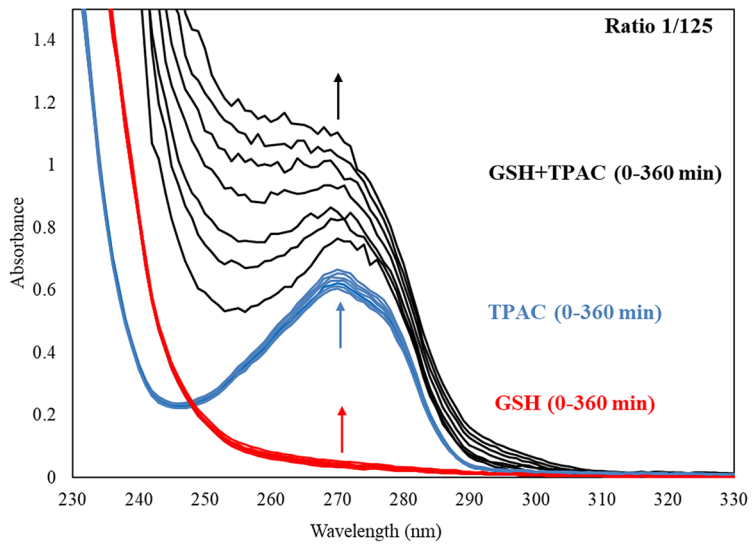

(C)

Fig. 8 UV spectra of the solutions containing **TPAC**, 33 (**A**), 66 (**B**) and 132 (**C**) µM in 100 mM Tris–HCl, pH = 7.4 with a high excess of GSH (16.5 mM) (1:500, 1:250 or 1:125 **TPAC**: GSH molar ratio, respectively) at 37 °C and after 1–6 h with 1-h interval

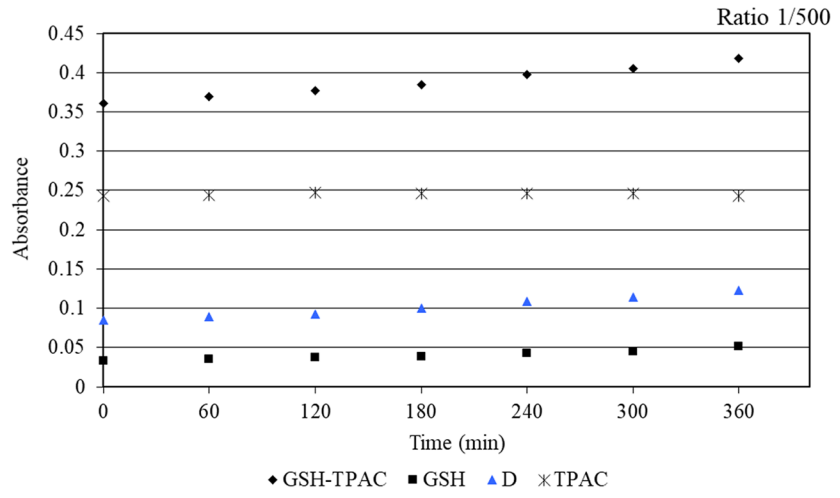

(A)

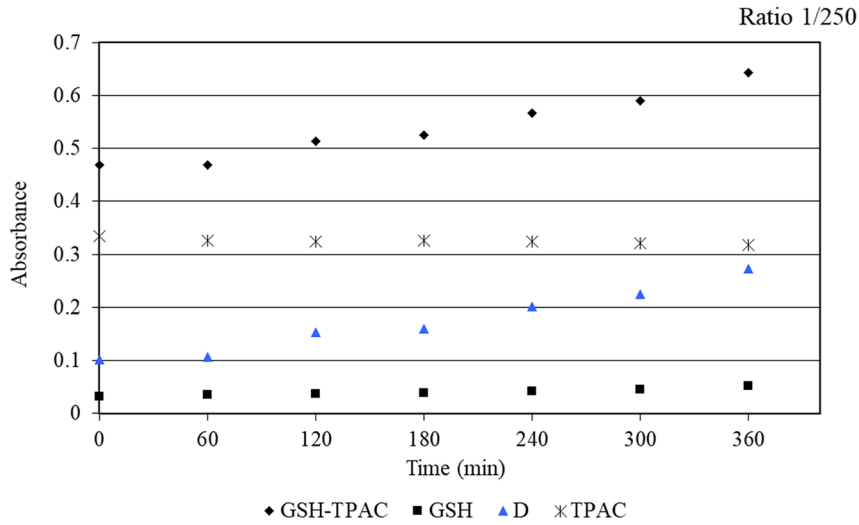

(B)

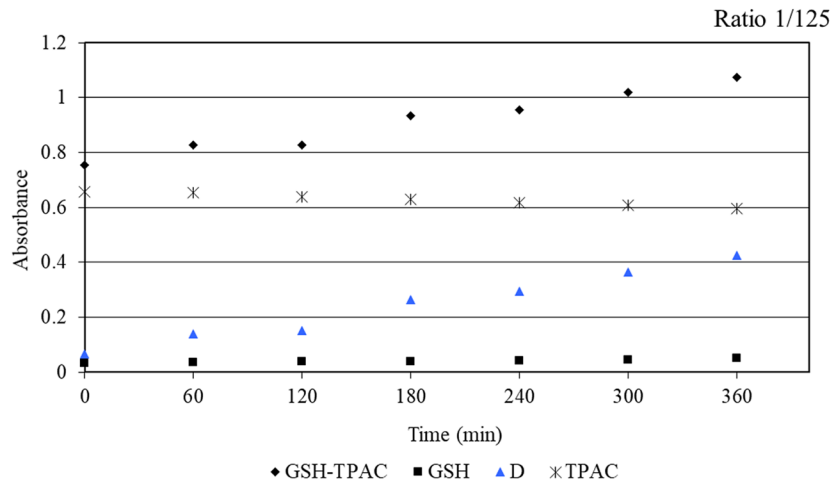

(C)

Fig. 9 Absorbance at 270 nm of GSH (16.5 mM) incubated with **TPAC** 33 (A), 66 (B) and 132 µM (C) in 100 mM Tris–HCl, pH 7.4, buffer containing 5 mM NaCl at 370C vs time (0–6 h) (◆), GSH (■), **TPAC** (Ж) and the points derived from the subtraction among them (D) curve (▲)

Table 2 Initial rates of the reactions between **TPAC** and GSH obtained from UV absorption data at 270 nm as a function of time (0–360 min)

TPAC (μM)	GSH (mM)	Initial slope × 10^3 (min^{-1})	R^2	Refs.
132	16.5	0.9394	0.94	*
66	16.5	0.3415	0.95	*
33	16.5	0.0701	0.98	*
Cisplatin (μM) [15]				
99	16.5	1.4640	0.99	[15]
66	16.5	0.7981	0.99	[15]
33	16.5	0.3635	0.99	[15]

The differences were fitted to the equation: $I_d = C + A_1\exp(-b_1 t) + A_2\exp(-b_2 t)$, while the initial slope (S_o) was calculated as $-(A_1b_1 + A_2b_2)$

*Present work

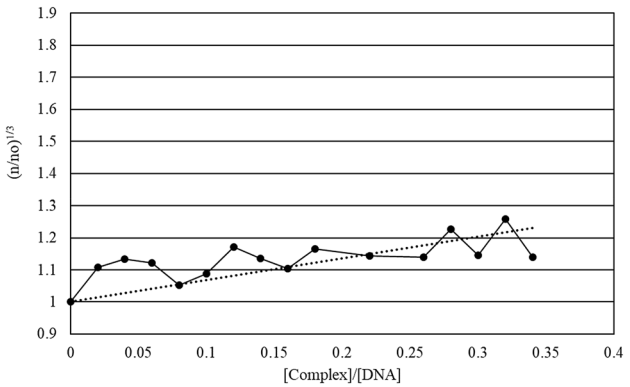

Fig. 10 Relative viscosity of CT-DNA with increasing concentrations of **TPAC** ([DNA] = 10 mM, r = [compound]/[DNA], *n* is the viscosity of DNA in the presence of the metallodrug and n_o is the viscosity of DNA alone)

by Dabrowiak, et.al [48]. The difference curve is fitted to the equation: $I_d = C + A_1\exp(-b_1 t) + A_2\exp(-b_2 t)$ and the initial reaction slope (So) is then derived from the equation $So = -(A_1b_1 + A_2b_2)$ [13]. Table 2 summarizes the results for **TPAC**. The order of the reaction towards a metallotherapeutic agent is calculated by the equation $So_i = k\,[complex]_i^x$ and alternatively from the ln(So) vs ln([complex]) graph (Table 2). The x value shows that the reaction is of first order towards **TPAC**. GSH involves in cisplatin resistance of tumor cells by reacting with it in a first order reaction similarly to that of **TPAC** with GSH (Table 2) [15].

DNA solution viscosity measurements: Relative viscosity measurements have proven to be a reliable method to assign the mode of binding of metal compounds with DNA [49]. The DNA length changes upon incubation with a metallodrug, affecting the viscosity of its solution. Thus, the binding mode is distinguished since covalent and non-covalent binding display different characteristics [50]. In the case of intercalation of the agent between DNA bases, the relative viscosity of solution of DNA with metal compound is increased, due to the unwinding and elongation of the double helix [49]. In the case that a metallodrug interacts electrostatically with the DNA, no effect on DNA length is caused and no significant change of the viscosity is observed. In the case of DNA strand cleavage by an agent, the length of the DNA decreases and the viscosity decreases significantly as well [50].

Solution of CT-DNA (10 mM) is incubated with increasing amounts of **TPAC** in the molar ratio up to $r = 0.35$ [compound]/[DNA]. Figure 10, shows the relative specific viscosity $(\eta/\eta_0)^{1/3}$ vs binding ratio. The compound **TPAC** increases the relative viscosity of DNA similarly to the ethidium bromide [49], indicating that **TPAC** intercalates to DNA strands [50].

Fluorescence spectroscopic studies: Ethidium bromide (EB) is a classical intercalator. EB gives significant fluorescence emission intensity when it intercalates into the basis pairs of DNA [51]. Since EB intercalates to DNA, its replacement from a quencher, leads to quenching of the fluorescence emitted. Therefore, an intercalation binding mode of the agent towards DNA is concluded [15, 20, 23, 40]. Excitation of the CT-DNA–EB complex at $\lambda_{ex} = 527$ nm emits at $\lambda_{max} = 588$ nm. The fluorescence spectra of the CT-DNA–EB complex with increasing concentrations of **TPAC** (0–600 μM) are shown in Fig. 11. The fluorescence undergoes quenching by 65.3% when the CT-DNA–EB was treated with **TPAC** at 600 μM. The intercalative binding mode of TPAC to DNA which is observed by fluorescence spectroscopy agrees with that of DNA solution viscosity measurements above.

The apparent formation constant K_{app} of the DNA-quencher is calculating by the equation

$$K_{app} = K_{EB} \times [EB]/[Q_{50}],$$

where $[Q_{50}]$ is the quencher concentration at the 50% reduction of the fluorescence, $K_{EB} = 10^7\ M^{-1}$, and [EB] = 2.3 μM [15, 20, 23, 40]. The Stern–Volmer quenching constant (K_{SV}) of the EB–DNA complex is calculated from the slope of the line derived from the diagram of I_0/I vs the concentration of the complex [Q] [15, 20, 23, 40] (Fig. 11). The K_{SV} value of **TPAC** is $(1.3 \pm 0.2) \times 10^3\ M^{-1}$, while the K_{app} value is $(31.0 \pm 4.3) \times 10^3\ M^{-1}$.

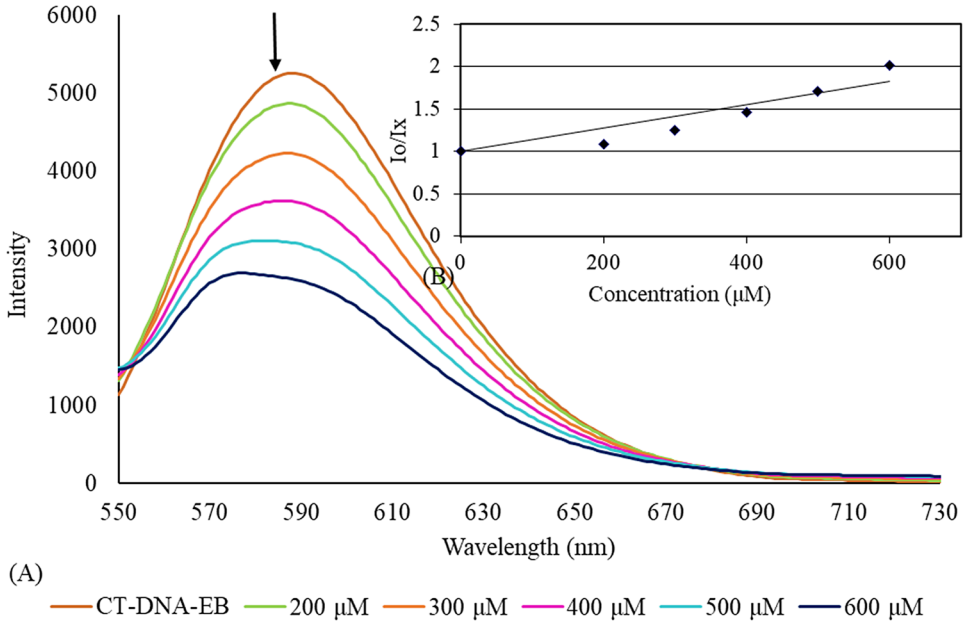

Fig. 11 **A** Emission spectrum of CT-DNA–EB complex in the presence of **TPAC** ([EB] = 2.3 μM [DNA] = 26 μM [complex] = 0–600 μM) λ_{ex} = 527 nm). The arrow shows the intensity changing upon increasing complex concentration. **B** Inset shows the plots of emission intensity Io/I vs [complex]

Conclusions

GSH, a cysteine containing tripeptide, is over-expressed in the cancer cells. It takes place in the development of cancer cells resistance against chemotherapeutics, by reacting with the anti-cancer drugs of the cytoplasm. It removes metal ions from the cytoplasm towards extracellular space, preventing its effective interaction with crucial intracellular components (DNA, mitochondrion, etc.). However, GSH can readily reduce antimony(V) to highly toxic antimony(III). This defence mechanism of cancer cells against chemotherapy, can be used as a tool for activating a Sb(V) pro-drug inside the cytoplasm of cancer cells, selectively. For this, the organoantimony(V) derivative *trans*-O,O-[$Ph_3Sb(Carv)_2$] (**TPAC**) of carvacrol (CarvH), a natural product ingredient and a potent antitumor drug against metastatic breast cancer cells, is synthesized. The crystal structure of **TPAC** is the first example of metal complex where carvacrol is covalently bonded to the metal center.

TPAC inhibits breast human MDA-MB-231 (HI) cells stronger than cisplatin. It is similarly effective against both MCF-7 (HD) and MDA-MB-231 (HI) cells suggesting no involvement of hormone receptors in its mechanism of action. Moreover, **TPAC** potently inhibits both tumor cell lines, than the normal one. Since GSH reacts with **TPAC** to form the disulfide GS-SG, in a first order reaction in respect to the oxidizing agent with the consequent reduction of the Sb(V) to Sb(III), ex vivo, the selectivity towards cancer cell might attribute to a similar interference of **TPAC** in the cytoplasm of the cancer cells.

The morphology of MCF-7 cells incubated with **TPAC**, the DNA fragmentation and the Acridine Orange/Ethidium Bromide (AO/EB) staining reveal that the compound induces apoptosis. Cell cycle arrest study concludes that **TPAC** suppresses the cell proliferation by DNA synthesis inhibition. Moreover **TPAC** causes mitochondrion membrane integrity damage. Therefore the intrinsic apoptotic pathway, might initiate the cell death. Ex vivo studies have shown that **TPAC** intercalates with the DNA strands. Among the antimony(V) compounds of natural products ingredients ($SalH_2$ and carvacrol), **TPAC** exhibits greater activity than {[$Ph_3Sb(SalH)]_2O$} against cancer cells.

Experimental

Materials and instruments: All used solvents were of reagent grade, triphenyl antimony, carvacrol, dimethylsulfoxide (DMSO, Riedel-de Haën) were used without any further purification. Dulbecco's modified Eagle's medium, (DMEM), fetal bovine serum, glutamine and trypsin were purchased from Gibco, Glasgow, UK. Phosphate buffer saline (PBS), CT-DNA, ethidium bromide, propidium iodide, Triton X-100, agarose, ethylenediaminetetraacetic acid (EDTA), RNase A, Proteinase K were purchased from Sigma-Aldrich. Dimethyl sulfoxide was from Riedel–de Haen. Melting point was measured in open tubes with Stuart Scientific apparatus and it is uncorrected. Mid-infrared spectra (4000–400 cm^{-1}) were obtained on Cary 670 FTIR spectrometer (Agilent Technologies). A UV-1600 PC series spectrophotometer of VWR was used for the recording of electronic absorption spectra. The fluorescence spectra were recorded on a Jasco FP-8200 Fluorescence Spectrometer. Thermal studies were carried out on a a DTG/TG NETZSCH

STA 449C apparatus, under air flow (with a heating rate of 10 °C min^{-1} (25–500 °C). FACS Calibur flow cytometer (Becton Dickinson, San Jose, CA, USA) was used for the cell cycle arrest experiments.

*Synthesis and crystallization of **TPAC**:* **TPAC** was synthesized by the oxidation 0.176 g Ph_3Sb^{III} (0.5 mmol) with 0.05 ml H_2O_2 30% hydrogen peroxide in the presence of 153 µL of CarvH (1 mmol) in 15 mL Et_2O. The solution was stirred overnight and a white precipitation was filtered off and dries in vacuum over calcium dichloride. Colorless crystals of **TPAC** suitable for X-ray analysis were grown from a methanol/acetonitrile solution (10:10 ml).

TPAC: Colorless crystal, melting point: 105–110 °C;. IR (cm^{-1}): 3062w, 2952 s, 2920w, 2863w, 1601 s, 1570 s, 1494 s, 1478w, 1456w, 1434 s, 1412 s, 1330 s, 1305w, 1251vs, 1178 s, 1125 s, 1068 s, 1021w, 992 s, 938 s, 875 s, 850 s, 812 s, 768 s, 730vs, 715w, 689vs, 615 s, 619 s, 522 s, 456vs, 436w, 421w, UV–vis (DMSO): λ = 277 nm (logε = 3.72).

X-ray fluorescence spectroscopy: XRF measurement was carried out using an Am-241 radioisotopic source (exciting radiation 59.5 keV). For the detection of X-ray fluorescence a Si (Li) detector was used. The measuring time was chosen so as to collect ~ 2000 data on the weaker Kα peak. XRF measurement was also carried out with Rigaku NEX QC EDXRF analyzer, (Austin, TX, USA).

X-ray structure determination: A crystal with approximate dimensions 0.03 × 0.03 × 0.33 mm was taken from the mother liquor and immediately cooled to − 113 °C. Diffraction measurements were made on a Rigaku R-AXIS SPIDER Image Plate diffractometer using graphite monochromated Mo Kα radiation. Data collection (ω-scans) and processing (cell refinement, data reduction and Empirical absorption correction) were performed using the CrystalClear program package [52]. Important crystallographic data are listed below. The structure was solved by direct methods using SHELXS v.2013/1 and refined by full-matrix least-squares techniques on F2 with SHELXL ver.2014/6 [53, 54]. Further experimental crystallographic details: 2θmax = 48°; reflections collected/unique/used, 42,099/10315 [R_{int} = 0.1739]/10315; 739 parameters refined; $(\Delta/\sigma)_{max}$ = 0.001; $(\Delta\rho)_{max}/(\Delta\rho)_{min}$ = 0.784/− 1.175 e/Å^3; R1/wR2 (for all data), 0.1314/0.1401. All hydrogen atoms were introduced at calculated positions as riding on bonded atoms. All non-hydrogen atoms were refined anisotropically. Plots of the structure were drawn using the Diamond 3 program package [55].

TPAC: $C_{38}H_{41}O_2Sb$, MW = 651.47 g/mol, triclinic, space group P-1 space group with a = 8.8667(4) Å, b = 19.3885(8) Å, c = 20.0125(10) Å, α = 100.763(2)°, β = 99.855(2)°, γ = 96.293(1)°, V = 3294.2(3) Å^3, Z = 4, T = 160 K, Radiation Mo Kα, ρ(calc) = 1.314 g cm^{-3}, μ = 0.868 mm^{-1}, Reflections with $I > 2\sigma(I)$ = 5873, $R_1{}^a$ = 0.0634 ($^aR_1 = \Sigma(|F_o|-|F_c|)/\Sigma(|F_o|)$ and $wR_2 = \{\Sigma[w(F_o{}^2-F_c{}^2)^2]/\Sigma[w(F_o{}^2)^2]\}^{1/2}$), $wR_2{}^a$ = 0.1135 ($w = 1/[\sigma^2(F_o{}^2)+(\alpha P)^2+bP]$ and $P = [\max(F_o{}^2,0)+2F_c{}^2]/3$, α = 0.0388, b = 1.8996).

While the quality of the structural analysis is not as high as expected for a crystallographic work, the unambiguous establishment of the molecular connectivity is what the need of the present work demands. The R value of 0.0634 and the good reflection to parameter ratio (higher than ten) are quiet good conditions to support publication. Few crystals were tested but all were poorly diffracting, probably because of their shape, i.e., very thin needles. For the one finally chosen to be measured a very long measuring time (27 min/scan) was used and a quite low temperature.

Crystallographic data (excluding structure factors) for the structures reported in this paper have been deposited with the Cambridge Crystallographic Data Centre as supplementary publication no. CCDC- 2,119,381. Copies of the data can be obtained free of charge on application to CCDC, 12 Union Road, Cambridge CB2 1EZ, UK (fax: (+ 44) 1223-336-033; e-mail: deposit@ccdc.cam.ac.uk).

Biological tests

Solvents used: The biological experiments including assessment of viability with SRB assay micronucleus, cell morphology studies, cell cycle arrest, Acridine Orange/Ethidium Bromide (AO/EB) Staining and permeabilization of the mitochondrial membrane test were carried out using stock solution of **TPAC** (0.01 M) in DMSO, solution of cisplatin in double distil water (0.08 M), solution of carvacrol in DMEM (0.01 M) and solution of Ph_3Sb in DMSO (0.01 M). Stock solutions of **TPAC**, cisplatin and Ph_3Sb were freshly prepared and diluted with cell culture media to the desired concentration. For DNA-binding studies, the experiments were carried in buffer solution.

Sulforhodamine B (SRB) assay: This study was performed according to the procedure reported previously [15, 40]. Briefly, cells were plated (100 µL per well) in 96-well flat-bottom microplates at various cell inoculation densities (MCF-7, MDA-MB-231 and MRC-5: 6000, 8000 and 2000 cells/well, respectively). The cells cultures were incubated for 24 h at 37ºC to resume exponential growth and stabilization and then they were exposed to **TPAC** for 48 h (2–30 µM) by the addition of either 100 µL complete culture medium (control wells) or 100 µL of agent's solution at the final concentrations diluted in complete culture medium (test wells). The measurements are repeated twice in each plate. The evaluation of the cell viability under their treatment with TPAC was performed by the SRB colorimetric assay at λ = 568 nm, which gives the percent of the survive cells towards the control ones (untreated cells).

Evaluation of in vitro *genotoxicity with micronucleus assay*: The evaluation of genotoxicity caused by **TPAC** was

performed following the protocol reported elsewhere [40]. Briefly, MRC-5 cells were seeded (4×10^4 cells/well) in glass cover slips which were afterwards placed in six-well plates, with 3 mL of cell culture medium and incubated for 24 h. MRC-5 cells were, then, exposed into **TPAC** in its IC_{50} value for a period of 48 h. The cover slips were, after, washed three times with PBS and once with a hypotonic solution (75 mM KCl) for 10 min at room temperature. The hypotonized cells were fixed by at least three changes of acetic acid/methanol 1:3 solution. The cover slips were also washed with cold methanol containing 1% acetic acid. The cover slips were then stained with acridine orange (50 µg/mL) for 15 min at 37 °C. After, the cover slips were rinsed three times with PBS to remove any excess acridine orange. The number of micronucleated cells per 1000 cells was determined.

Cell morphology studies: MCF-7 cells morphology was observed under an inverse microscope, after incubation of MCF-7 cells by **TPAC**, for 48 h.

DNA fragmentation: The DNA fragmentation study was performed as reported previously [40, 56]. Briefly, MCF-7 cells were seeded at a density of 3×10^5 cells/well in 10 mm plates at 37 °C for 48 h. The cultures media were transferred to a test tube with the attached cells, which were washed twice with PBS and detached with a silicone spatula. The test tube was centrifuged at 3000 rpm for 10 min and the supernatant has been removed. The cell pellets were re-suspended in 1 mL PBS, transferred to a micro-tube and centrifuged at 3000 rpm for 15 min and the supernatant has also been removed again. In micro-tube 100 µL of lysis buffer, consisting of 0.5% Triton X-100, 0.01 M Tris–HCl pH = 7.4 and 0.01 M EDTA pH = 8, was added and it was incubated on ice bath for 30 min. The lysate was centrifuged at 12,000 rpm for 30 min. The supernatant was then transferred to a micro-tube and incubated with 2 µL of RNase A (10 mg mL^{-1}) for 2 h at 37 °C and then with 2.5 µL of Proteinase K (20 mg mL^{-1}) for 2 h at 37 °C. DNA from the supernatant was precipitated overnight at − 20 °C via the addition of 20 µL of 5 M NaCl and 120 µL of isopropyl alcohol. The micro-tube was centrifuged at 6000 rpm for 90 min, air-dried, and re-suspended in 20 µL of TE buffer, at pH = 7.4, consisting of 0.01 M Tris–HCl, pH = 7.4, and 0.001 M EDTA, pH = 8. A loading buffer, which contained 50% glycerol and 0.001 M EDTA, pH = 8, was then added to the samples at a ratio of 1:10 (v/v). Electrophoresis was performed on 1.6% agarose gel in TBE containing 1 μgml^{-1} ethidium bromide, for 60 min at 40 V. The DNA was visualized under ultraviolet light. The λ HindIII DNA Ladder was used as ladder.

Cell cycle arrest: This study was performed as previously reported [40]. Briefly, MCF-7 cells were seeded at a density of 1×10^5 cells/well in six-well plates at 37 °C for 24 h. The cells were treated with **TPAC** at its IC_{50} value and they were incubated for 48 h. The cells were trypsinized, washed twice with PBS and separated by centrifugation, afterwards. The cells were incubated overnight at − 20 °C following the addition of 1 mL of cold 70% ethanol. For analysis, the cells were centrifuged, transferred into PBS, incubated with RNase (0.2 mg/mL) and propidium iodide (0.05 mg/mL) for 40 min at 310 K, and then analyzed by flow cytometry. For each sample, 10,000 events were recorded. The resulting DNA histograms were drawn and quantified using the FlowJo software (version FlowJo X 10.0.7r2).

Acridine Orange/Ethidium Bromide (AO/EB) staining to detect apoptosis: The MCF-7 cells were seeded into a 24-well plate (70,000 cells per well) and cultured at 37 °C in a CO_2 incubator for 24 h. Afterwards, the cells were treated with TPAC at its IC_{50} value for 48 h. Control and treated cells were collected after 48 h, the cells were harvested, washed twice with PBS and centrifuged. 25 µL of cell suspension in PBS were incubated with 50 µgr/mL AO and 50 µgr/mL EB solution. Then, the cells were mixed gently and 10 µL of cells in suspension was placed on a glass slide and a cover slip was placed over it. At random, 300 cells were immediately observed in a fluorescent microscope (Optika inverted fluorescence microscope) and examined at × 60 magnification. The percentage of cells reflecting pathological changes was calculated [20, 23].

Permeabilization of the mitochondrial membrane test: The permeabilization of the mitochondrial membrane test (MMP assay) was performed using the kit which was purchased from sigma Aldrich "Mitochondria Membrane Potential Kit for Microplate Readers, MAK147". MCF-7 cells were treated with TPAC at its IC_{50} value. The fluorescence intensity is measured at $\lambda_{ex} = 540$ and $\lambda_{em} = 590$ nm. The experimental outputs include only intensities of fluorescence of the solutions (2 solutions of treated cells in wells and 2 solutions of untreated cells in wells) [40].

*Order of the reaction of **TPAC** with GSH as monitored by UV spectroscopy:* Stock solutions of **TPAC** (0.01 M) in DMSO and GSH (0.08 M) in double-distilled water were used for the experiment. Three solutions of **TPAC** (33, 66 and 132 µM) were prepared from dilution from the stock one using buffer 100 mM Tris–HCl and 5 mM NaCl, pH 7.4. The concentration of GSH was maintained at 16.5 mM (1/500, 1/250 and 1/125 glutathione/compound molar ratios). The temperature of the reaction mixture was kept at 37 °C. To exclude the influence of the disulfide formed by the oxidation of GSH the UV spectra of the GSH solution without **TPAC** was recorded for the same reaction period [48, 57]. The difference curve ($Abs_{compound\text{-}GSH}$—$Abs_{GSH}$- Abs_{comp}) is fitted to the equation $I_d = C + A_1 \exp(-b_1 t) + A_2 \exp(-b_2 t)$ and the initial reaction slope is then derived from the equation $So = -(A_1 b_1 + A_2 b_2)$. The order of the reaction (x) is calculated from the equation $So_i = k\,[complex]_i^x$ [48, 57].

DNA-binding studies

Viscosity measurements: This study was carried out as previously reported [58]. The kinematic viscosity of DNA solutions with or without **TPAC** (0–0.35 [**TPAC**]/[DNA] molar ratios) was measured with an Ostwald-type viscometer.

Fluorescence studies: The emission spectra at 588 nm of EB (2.3 μM) solutions that contain CT-DNA (26 μM) in the absence or presence of various concentrations of TPAC (0–600 μM) were recorded upon their excitation at 527 nm.

Supplementary Information The online version contains supplementary material available at https://doi.org/10.1007/s00775-022-01936-5.

Acknowledgements This work was carried out in fulfilment of the requirements for the Master thesis of Ms M.K. according to the curriculum of the International Graduate Program in "Biological Inorganic Chemistry", which operates at the University of Ioannina within the collaboration of the Departments of Chemistry of the Universities of Ioannina, Athens, Thessaloniki, Patras, Crete and the Department of Chemistry of the University of Cyprus (http://bic.chem.uoi.gr/BIC-En/index-en.html) under the supervision of Prof. S.K.H. C.N.B. has been financially supported by the State Scholarships Foundation (ΙΚΥ) (Project No. 2019-050-0503-17816), through the Operational Programme "Human Resources Development, Education and Lifelong Learning" in the context of the project "Reinforcement of Postdoctoral Researchers—2nd Cycle" (MIS-5033021), which is co-financed by Greece and the European Union (European Social Fund- ESF). S.K.H. acknowledges the Oncology Department of Novartis Hellas S.A.C.I. for the financial support (Project No. 82819). The COST Action CA17104 "New diagnostic and therapeutic tools against multidrug resistant tumors" members are acknowledged for the stimulating discussions. This research has been co-financed by the European Union and Greek national funds through the Operational Program Competitiveness, Entrepreneurship and Innovation, under the call RESEARCH – CREATE – INNOVATE (project code:T1EDK-02990).

Author contributions Conceptualization, SKH; Investigation, MK, CNB, CP, VP and CPR; Methodology, CNB and SKH; Supervision, SKH; Validation, SKH; Writing-Original Draft, CNB and SKH; Writing—Review and Editing, CNB and SKH. All authors have read and agreed to the published version of the manuscript.

Declarations

Conflict of interest There are no conflicts to declare.

References

1. Khan I, Bahuguna A, Kumar P, Bajpai VK, Chul Kang S (2018) In vitro and in vivo antitumor potential of carvacrol nanoemulsion against human lung adenocarcinoma A549 cells via mitochondrial mediated apoptosis. Sci Rep 8:144–158
2. Friedman M (2014) Chemistry and multibeneficial bioactivities of carvacrol (4-Isopropyl-2-methylphenol), a component of essential oils produced by aromatic plants and spices. Agric Food Chem 62:7652–7670
3. Arunasree KM (2010) Anti-proliferative effects of carvacrol on a human metastatic breast cancer cell line, MDA-MB231. Phytomedicine 17:581–588
4. Ozturk II, Hadjikakou SK, Hadjiliadis N, Kourkoumelis N, Kubicki M, Baril M, Butler IS, Balzarini J (2007) Synthesis, structural characterization and biological studies of new antimony(III) complexes with thioamides. The influence of the solvent on the geometry of the complexes. Inorg Chem 46:8652–8661
5. Ozturk II, Hadjikakou SK, Hadjiliadis N, Kourkoumelis N, Kubicki M, Tasiopoulos AJ, Scleiman H, Barsan MM, Butler IS, Balzarini J (2009) New Antimony(III) bromide complexes with thioamides: synthesis, characterization, and cytostatic properties. Inorg Chem 48:2233–2245
6. Ozturk I, Filimonova S, Hadjikakou SK, Kourkoumelis N, Dokorou V, Manos E, Tasiopoulos AJ, Barsan MM, Butler IS, Milaeva ER, Balzarini J, Hadjiliadis N (2010) Structural motifs and biological studies of new antimony(III) iodide complexes with thiones. Inorg Chem 49:488–501
7. Gkaniatsou EI, Banti CN, Kourkoumelis N, Skoulika S, Manoli M, Tasiopoulos AJ, Hadjikakou SK (2015) Novel mixed metal Ag(I)-Sb(III)-metallotherapeutics of the NSAIDs, aspirin and salicylic acid: Enhancement of their solubility and bioactivity by using the surfactant CTAB. J Inorg Biochem 150:108–119
8. Hadjikakou SK, Ozturk II, Banti CN, Kourkoumelis N, Hadjiliadis N (2015) Recent advances on antimony(III/V) compounds with potential activity against tumor cells. J Inorg Biochem 153:293–305
9. Sharma P, Perez D, Cabrera A, Rosas N, Arias JL (2008) Perspectives of antimony compounds in oncology. Acta Pharmacol Sinm 29:881–890
10. Ozturk II, Banti CN, Manos MJ, Tasiopoulos AJ, Kourkoumelis N, Charalabopoulos K, Hadjikakou SK (2012) Synthesis, characterization and biological studies of new antimony(III) halide complexes with ω-thiocaprolactam. J Inorg Biochem 109:57–65
11. Ozturk II, Urgut OS, Banti CN, Kourkoumelis N, Owczarzak AM, Kubicki M, Hadjikakou SK (2014) Synthesis, structural characterization and cytostatic properties of N, N-dicyclohexyldithiooxamide complexes of antimony(III) Halides (Sb_X3, X: Br or I). Polyhedron 70:172–179
12. Urgut OS, Ozturk II, Banti CN, Kourkoumelis N, Manoli M, Tasiopoulos AJ, Hadjikakou SK (2016) New antimony(III) Halide complexes with dithiocarbamate ligands derived from thiuram degradation: the effect of the molecule's close contacts on in vitro cytotoxic activity. Mater Sci Eng C 58:396–408
13. Ozturk II, Yarar S, Banti CN, Kourkoumelis N, Chrysouli MP, Manoli M, Tasiopoulos AJ, Hadjikakou SK (2017) QSAR studies on antimony(III) halide complexes with N-substituted thiourea derivatives. Polyhedron 123:152–161
14. Syng-Ai C, Leela Kumari A, Khar A (2004) Effect of curcumin on normal and tumor cells: Role of glutathione and bcl-2. Mol Cancer Ther 3:1101–1108
15. Banti CN, Kyros L, Geromichalos GD, Kourkoumelis N, Kubicki M, Hadjikakou SK (2014) A novel silver iodide metalo-drug: Experimental and computational modelling assessment of its interaction with intracellular DNA, lipoxygenase and glutathione. Eur J Med Chem 77:388–399
16. Gielen M (1992) Metal-based anti-tumour drugs, vol 2. Freund Publ House Ltd, London
17. Wang GC, Lu YN, Xiao J, Yu L, Song HB, Li JS, Cui JR, Wang RQ, Ran FX (2005) Synthesis, crystal structures and in vitro antitumor activities of some organoantimony arylhydroxamates. J Organomet Chem 690:151–156
18. Ozturk II, Banti CN, Kourkoumelis N, Manos MJ, Tasiopoulos AJ, Owczarzak AM, Kubicki M, Hadjikakou SK (2014) Synthesis, characterization and biological activity of antimony(III) or bismuth(III) chloride complexes with dithiocarbamate ligands derived fromthiuram degradation. Polyhedron 67:89–103
19. Chrysouli MP, Banti CN, Kourkoumelis N, Panayiotou N, Tasiopoulos AJ, Hadjikakou SK (2018) Chloro(triphenylphosphine) gold(I) a forefront reagent in gold chemistry as apoptotic agent for cancer cells. J Inorg Biochem 179:107–120

20. Banti CN, Raptopoulou CP, Psycharis V, Hadjikakou SK (2021) Novel silver glycinate conjugate with 3D polymeric intermolecular self-assembly architecture; an antiproliferative agent which induces apoptosis on human breast cancer cells. J Inorg Biochem 216:111351
21. Banti CN, Tsiatouras V, Karanicolas K, Panagiotou N, Tasiopoulos AJ, Kourkoumelis N, Hadjikakou SK (2020) Antiproliferative activity and apoptosis induction, of organo-antimony(III)–copper(I) conjugates, against human breast cancer cells. Mol Divers 24:1095–1106
22. Poyraz M, Demirayak S, Banti CN, Manos MJ, Kourkoumelis N, Hadjikakou SK (2016) Platinum(II)-thiosemicarbazone metal-drugs override the cell resistance due to glutathione; assessment of their activity against human adenocarcinoma cells. J Coord Chem 69:3560–3579
23. Stathopoulou MEK, Zoupanou N, Banti CN, Douvalis AP, Papachristodoulou C, Marousis KD, Spyroulias GA, Mavromoustakos T, Hadjikakou SK (2021) Organotin derivatives of cholic acid induce apoptosis into breast cancer cells and interfere with mitochondrion; Synthesis, characterization and biological evaluation. Steroids 167:108798
24. Banti CN, Hadjikakou SK, Sismanoglu T, Hadjiliadis N (2019) Anti-proliferative and antitumor activity of organotin(IV) compounds. An overview of the last decade and future perspectives. J Inorg Biochem 194:114–152
25. Gu X-F, Zhao Y, Li K, Su M-X, Yan F, Li B, Du Y-X, Di B (2016) Differentiation of volatile aromatic isomers and structural elucidation of volatile compounds in essential oils by combination of HPLC separation and crystalline sponge method. J Chromatogr A 1474:130–137
26. Balestri D, Mazzeo PP, Perrone R, Fornari F, Bianchi F, Careri M, Bacchi A, Pelagatti P (2021) Deciphering the supramolecular organization of multiple guests inside a microporous MOF to understand their release profile. Angew Chem Int Ed 60:10194–10202
27. Pasch R, Koelle U, Ganter B, Englert U (1997) Planar Chiral Cp*Ru Complexes. 2.1 Bis(allyl) and -(arene) complexes derived from (R)-Carvone. Organometallics 16:3950–3958
28. Xanthopoulou MN, Hadjikakou SK, Hadjiliadis N, Kubicki M, Karkabounas S, Charalabopoulos K, Kourkoumelis N, Bakas T (2006) Synthesis and characterization of a new chloro-diphenyltin(IV) complex with thioamide 2-mercapto-nicotinic acid. Study of its influence upon the catalytic oxidation of linoleic acid to hydroperoxylinoleic acid by the enzyme Lipoxygenase. J Organomet Chem 691:1780–1789
29. Addison AW, Rao TN, Reedijk J, Van Rijn J, Verschoor GC (1984) Synthesis, structure, and spectroscopic properties of Copper(II) compounds containing nitrogen-sulphur donor ligands; the crystal and molecular structure of Aqua[l,7-bis(N-methylbenzimidazol-2'-yl)- 2,6-dithiaheptane]copper(ii) Perchlorate. J Chem Soc Dalt Trans 7:1349–1356
30. Sharutin VV, Sharutina OK, Efremov AN (2016) Synthesis and structure of tri(p-tolyl)antimony diaroxides. Russ J Gen Chem 86:1212
31. Sharutin VV, Sharutina OK, Efremov AN (2017) Tris(para-tolyl)- and tris(4-fluorophenyl)antimony diaroxides: syntheses and structures. Koord Khim (Russ) (Coord Chem) 43:565–572
32. Sharutin VV, Sharutina OK, Senchurin VS (2016) Synthesis and structure of bis(4-iodophenoxy)triphenylantimony and 4-iodophenoxytetraphenylantimony. Russ Chem Bull 65:751
33. Sharutin VV, Pakusina AP, Subacheva OV, Sharutina OK, Gerasimenko AV (2003) Synthesis and structure of diphenoxytriphenylantimony. Koord Khim (Russ) (Coord. Chem) 29:418–423
34. Poddelsky AI, Somov NV, Kurskii YuA, Cherkasov VK, Abakumov GA (2008) Hexacoordinate triphenylantimony(V) complex with tridentate bis-(3,5-di-tert-butyl-phenolate-2-yl)-amine ligand: Synthesis, NMR and X-ray study. J Organomet Chem 693:3451–3455
35. Chambre DR, Moisa C, Lupitu A, Copolovici L, Pop G, Copolovici D-M (2020) Chemical composition, antioxidant capacity, and thermal behavior of Satureja hortensis essential oil. Sci Rep 10:21322
36. Dong S, Dou X, Mohan D, Pittman CU Jr, Luo J (2015) Synthesis of graphene oxide/schwertmannite nanocomposites and their application in Sb(V) adsorption from water. Chem Eng J 270:205–214
37. Razandi M, Pedram A, Levin ER (2000) Plasma membrane estrogen receptors signal to antiapoptosis in breast cancer. Mol Endocrinol 14:1434–1447
38. Abughazaleh RD, Tracy TS (2014) In: Balakrishnan N, Colton T, Everitt B, Piegorsch W, Ruggeri F, Teugels JL (eds) Therapeutic Index. Wiley StatsRef: Stat. Ref. Online. https://doi.org/10.1002/9781118445112.stat07121
39. Polychronis NM, Banti CN, Raptopoulou CP, Psycharis V, Kourkoumelis N, Hadjikakou SK (2019) Non steroidal anti-inflammatory drug (NSAIDs) in breast cancer chemotherapy; antimony(V) salicylate a DNA binder. Inorg Chim Acta 489:39–47
40. Banti CN, Papatriantafyllopoulou C, Manoli M, Tasiopoulos AJ, Hadjikakou SK (2016) Nimesulide silver metallodrugs, containing the mitochondriotropic, triaryl derivatives of pnictogen; Anticancer activity against human breast cancer cells. Inorg Chem 55:8681–8696
41. Andiappan K, Sanmugam A, Deivanayagam E, Karuppasamy K, Kim H-S, Vikraman D (2018) In vitro cytotoxicity activity of novel Schiff base ligand–lanthanide complexes. Sci Rep 8:3054
42. Naqvi S, Mohiyuddin S, Gopinath P (2017) Niclosamide loaded biodegradable chitosan nanocargoes: an in vitro study for potential application in cancer therapy. R. Soc. Open Sci. 4:170611
43. Afsar T, Trembley J, Salomon C, Razak S, Khan MR, Ahmed K (2016) Growth inhibition and apoptosis in cancer cells induced by polyphenolic compounds of Acacia hydaspica: involvement of multiple signal transduction pathways. Sci Rep 6:23077
44. Jaksic Z (2012) Mechanisms of organotin-induced apoptosis. In: Pagliarani A, Trombetti F, Ventrella V (eds) Biochemical and biological effects of organotins. Bentham Science Publishers, Italy
45. Hanigan MH, Devarajan P (2003) Cisplatin nephrotoxicity: molecular mechanisms. Cancer Ther 1:47–61
46. Alves SL, Santos PLT, Russo SM, dos Santos TD, Gibara GA (2021) Antitumor effects of carvacrol and thymol: a systematic review. Front Pharmacol 12:1673
47. Shayani-Jama H, Nematollahi D (2010) Electrochemical evidences in oxidation of acetaminophen in the presence of glutathione and N-acetylcysteine. Chem Commun 46:409–411
48. Dabrowiak JC, Goodisman J, Souid A-K (2002) Kinetic study of the reaction of cisplatin with thiols. Drug Metab Dispos 30:1378–1384
49. Aguirre JD, Angeles-Boza AM, Chouai A, Pellois J-P, Turro C, Dunbar KR (2009) Live cell cytotoxicity studies: documentation of the interactions of antitumor active dirhodium compounds with nuclear DNA. J Am Chem Soc 131(32):11353–11360
50. Kellett A, Molphy Z, Slator C, McKee V, Farrell NP (2019) Molecular methods for assessment of non-covalent metallodrug–DNA interactions. Chem Soc Rev 48:971–988
51. Lazić D, Arsenijević A, Puchta R, Bugarčić ŽD, Rilak A (2016) DNA binding properties, histidine interaction and cytotoxicity

studies of water soluble ruthenium(II) terpyridine complexes. Dalton Trans 45:4633–4646
52. CrystalClear, Rigaku/MSC Inc, 2005 (The Woodlands Texas)
53. Sheldrick GM (2008) A short history of SHELX. Acta Crystallogr A 64:112–122
54. Sheldrick GM (2015) Crystal structure refinement with SHELXL. Acta Crystallogr C 71:3–8
55. DIAMOND – Crystal and Molecular Structure Visualization, Ver. 3.1, Crystal Impact, Rathausgasse 30, 53111, Bonn, Germany
56. Banti CN, Giannoulis AD, Kourkoumelis N, Owczarzak AM, Poyraz M, Kubicki M, Charalabopoulos K, Hadjikakou SK (2012) Mixed ligand–silver(I) complexes with anti-inflammatory agents which can bind to lipoxygenase and calf-thymus DNA, modulating their function and inducing apoptosis. Metallomics 4:545–560
57. Halamikova A, Heringova P, Kasparkova J, Intini FP, Natile G, Nemirovski A, Gibson D, Brabec V (2008) Cytotoxicity, mutagenicity, cellular uptake, DNA and glutathione interactions of lipophilic trans-platinum complexes tethered to 1-adamantylamine. J Inorg Biochem 102:1077–1089
58. Latsis GK, Banti CN, Kourkoumelis N, Papatriantafyllopoulou C, Panagiotou N, Tasiopoulos A, Douvalis A, Kalampounias AG, Bakas T, Hadjikakou SK (2018) Poly organotin acetates against DNA with possible implementation on human breast cancer. Int J Mol Sci 19:2055